HHS Public Access

Author manuscript

Biochemistry. Author manuscript; available in PMC 2020 October 20.

Published in final edited form as:

Biochemistry. 2020 October 13; 59(40): 3802–3812. doi:10.1021/acs.biochem.0c00690.

Protease Inhibition Mechanism of Camelid-like Synthetic Human Antibodies

Dong Hyun Nam[†], **Ki Baek Lee**[†], **Evan Kruchowy**, **Henry Pham**, **Xin Ge**

Department of Chemical and Environmental Engineering, University of California, Riverside, Riverside, California 92521, United States

Abstract

Macromolecular protease inhibitors and camelid single-domain antibodies achieve their enzymic inhibition functions often through protruded structures that directly interact with catalytic centers of targeted proteases. Inspired by this phenomenon, we constructed synthetic human antibody libraries encoding long CDR-H3s, from which highly selective monoclonal antibodies (mAbs) that inhibit multiple proteases were discovered. To elucidate their molecular mechanisms, we performed in-depth biochemical characterizations on a panel of matrix metalloproteinase (MMP)-14 inhibitory mAbs. Assays included affinity and potency measurements, enzymatic kinetics, a competitive enzyme-linked immunosorbent assay, proteolytic stability, and epitope mapping followed by quantitative analysis of binding energy changes. The results collectively indicated that these mAbs of convex paratopes were competitive inhibitors recognizing the vicinity of the active cleft, with their significant epitopes scattered across the north and south rims of the cleft. Remarkably, identified epitopes were the surface loops that were highly diverse among MMPs and predominately located at the prime side of the proteolytic site, shedding light on the mechanisms of target selectivity and proteolytic resistance. Substrate sequence profiling and paratope mutagenesis further suggested that mAb 3A2 bound to the active-site cleft in a canonical (substrate-like) manner, by direct interactions between $_{100h}$NLVATP$_{100m}$ of its CDR-H3 and subsites S1–S5′ of MMP-14. Overall, synthetic mAbs carrying convex paratopes can achieve efficient inhibition and thus hold great therapeutic promise for effectively and safely targeting biomedically important proteases.

Graphical Abstract

Corresponding Author: Xin Ge – Department of Chemical and Environmental Engineering, University of California, Riverside, Riverside, California 92521, United States; xge@engr.ucr.edu.

Complete contact information is available at: https://pubs.acs.org/10.1021/acs.biochem.0c00690

[†]**Author Contributions**

D.H.N. and K.B.L. contributed equally to this work.

Supporting Information

The Supporting Information is available free of charge at https://pubs.acs.org/doi/10.1021/acs.biochem.0c00690.

SDS–PAGE of purified Fabs (Figure S1), kinetics of binding of Fabs on cdMMP-14 (Figure S2), active cleft of MMP-14 (Figure S3), nTIMP-2-binding surface on cdMMP-14 (Figure S4), a competitive ELISA with GM6001 (Figure S5), production of cdMMP-14 alanine point mutants (Figure S6), additional exemplary results of a competitive ELISA (Figure S7), production of Fab 3A2 mutants (Figure S8), and biolayer interferometry results of Fab 3A2 mutants (Figure S9) (PDF)

The authors declare no competing financial interest.

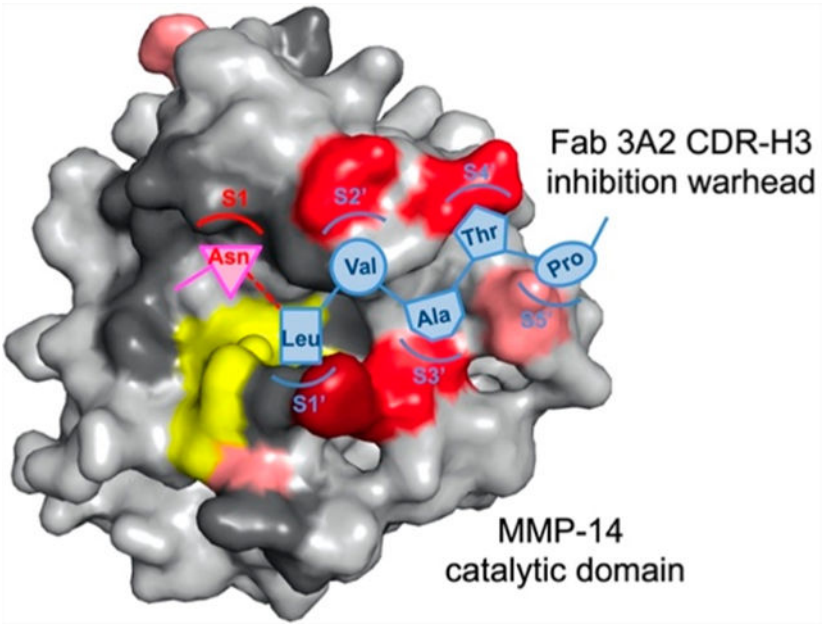

Accounting for ~2% of the human genome, proteases are important signaling molecules that precisely control a wide variety of physiological processes.[1–4] To maintain the body's homeostasis, proteases exist in a delicate balance of networks with their endogenous inhibitors and substrates. Altered protease expression or abnormal substrate proteolysis, therefore, causes many disorders ranging from inflammation,[5] cardiac diseases,[6] and cancer[7] to neuropathy,[8] degenerative diseases,[9] and osteoporosis.[10] In addition, numerous infectious diseases rely on proteases for the pathogen to invade the host cell,[11] replicate the viral genome,[12] process polyproteins,[13] and release progeny virions.[14] It is estimated that 5–10% targets for drug development are proteases.[15] One apparent therapeutic strategy is to block these abnormal or pathogenic proteolyses by inhibiting their catalytic reactions. Several protease inhibitors have been approved for the treatment of hypertension, coagulation, viral infection, cancer, and diabetes.[15] Nevertheless, despite decades of intensive effort, conventional drug discovery has achieved only limited success by targeting a small number of proteases.

Considering the vast proteolytic landscape and the levels of degradome complexity,[2,16] specificity is highly desired for any protease inhibition therapy. However, achieving target specificity can be difficult because proteolytic pathways often consist of highly homologous family members that share the same domain folding and catalytic chemistry.[17] Indeed, the main reasons why numerous matrix metalloproteinase (MMP) broad spectrum compound inhibitors, e.g., hydroxamates, all failed in clinical trials were a lack of efficacy and severe side effects caused by nonspecific inhibition of other metalloproteinases.[18–20] In contrast, monoclonal antibodies (mAbs) provide exquisite specificity capable of distinguishing between closely related protease family members.[21–34] Notably, among 569 human proteases identified, 279 (49%) are extracellular or pericellular, and thus can be accessed by therapeutic antibodies.[7]

Many naturally occurring protease inhibitors exhibit a convex-shaped conformation that inserts into the enzymatic active site and blocks substrate access and/or catalytic function.[35,36] However, from a molecular immunology perspective, the likelihood of generating antibodies with convex paratopes is low. In fact, active sites of enzymes have a low antigenicity for murine or human antibodies,[37] because the catalytic pocket is often buried inside a major cleft or concave structure and as such is inaccessible and/or incompatible with the antigen-binding surface topography of native human antibodies, often a cavity, groove, or flat surface but rarely a convex conformation. Intriguingly, a large proportion of antibodies isolated from camels and llamas bind the active-site pockets and efficiently inhibit enzymatic reactions.[37–39] However, camelid antibodies per se can evoke an immune response when administered to humans. In addition, these animals are usually not available for most researchers. To overcome these limitations, we designed and constructed synthetic human antibody libraries by incorporating enzyme-inhibiting paratopes inspired by camelid antibody repertoires into the human antibody scaffold.[33] Using these libraries, panels of nanomolar potent mAbs inhibiting multiple protease targets with high selectivity were identified.[33,34] Among these protease targets, MMP-14 is particularly important because of its roles in cancer progression and metastasis,[40,41] neuropathic pain,[42] and obesity.[43]

Our previous works have proven the concepts that convex library design and functional selection can facilitate the generation of inhibitory antibodies,[33,34] and their proteolytic stability, inhibitory potency, and selectivity can be further engineered.[44–46] This study aimed for in-depth characterizations of the inhibition mechanism of isolated anti-MMP14 Fabs (fragments antigen binding) that carry extended CDR-H3s. Numerous biochemical approaches were exploited, including enzymatic kinetics, a competitive enzyme-linked immunosorbent assay (ELISA), proteolytic stability, epitope alanine scanning, and calculation of free binding energy changes. As a result, the types of inhibition and important epitopes were identified for tested Fab inhibitors. Further analysis and paratope mutagenesis on the most potent Fab 3A2 revealed direct recognitions between its CDR-H3 and MMP-14 catalytic subsites. The likely mechanisms for high selectivity over other MMPs and proteolytic stability were also elucidated.

EXPERIMENTAL PROCEDURES

Preparation of Recombinant cdMMP-14 and Its Mutants.

The gene encoding the catalytic domain of MMP-14 (cdMMP-14, Tyr112–Pro290, UniProtKB P50281) was cloned via *Sfi*I sites into a periplasmic expression plasmid pMoPac16.[47] The obtained pMoPac16-cdMMP14 carried a *Lac* promoter, a *pelB* leader, and a C-terminal polyhistidine tag. Genes of cdMMP-14 site-directed alanine mutants were constructed by overlapping polymerase chain reaction (PCR) with mutagenic primers. Transformed *Escherichia coli* Jude-I cells [DH10B F′::Tn10 (Tet^r)] harboring cdMMP-14 wild type (wt) and mutants were grown in 2×YT medium supplemented with 34 μg/mL chloramphenicol at 30 °C for 16 h without addition of isopropyl β-D-1-thiogalactopyranoside.[48] The cells were harvested and treated with osmotic shocks to recover periplasmic fractions as described previously.[49] Briefly, 600 mL cell cultures were pelleted and resuspended in 60 mL of periplasmic buffer [200 mM Tris-HCl (pH 7.5), 20% sucrose, and

30 units/μL lysozyme] for incubation at room temperature for 10 min. The samples were then mixed with 60 mL of ice-cold doubly distilled H_2O followed by incubation on ice for 10 min. After centrifugation at 10000*g* for 30 min at 4 °C, cdMMP-14 wt and mutants were purified from periplasmic preparations by affinity chromatography using Ni-NTA agarose resin (Qiagen). The homogeneities of purified human cdMMP-14 wt and mutants were verified by sodium dodecyl sulfate–polyacrylamide gel electrophoresis (SDS–PAGE), and their concentrations were measured with a NanoDrop (Thermo Scientific).

Cloning, Expression, and Purification of Fabs and nTIMP-2.

V_H and V_L genes were cloned into the Fab expression vector containing a *PhoA* promoter, two STII leaders, and a polyhistidine tag at the C-terminus of the heavy chain.[50] V_H genes of 3A2 site-directed mutants were assembled by overlapping extension PCR and cloned in the same way. After expression in *E. coli* BL21 at 30 °C overnight in 2×YT medium, Fabs were purified from the periplasmic fractions by Ni-NTA chromatography and dialyzed against 50 mM HEPES and 150 mM NaCl (pH 6.8). The N-terminal domain of tissue inhibitor metalloproteinase-2 (nTIMP-2, UniProtKB P16035) was produced by *E. coli* periplasmic expression and affinity purified as described previously.[51] Purified proteins were analyzed by SDS–PAGE, and their concentrations were determined.

Biolayer Interferometry.

Purified cdMMP-14 wt was biotinylated by using the EZ-Link Sulfo-NHS-LC kit and then purified following the manufacturer's instructions (Pierce). Biotinylated cdMMP-14 (100 nM) was loaded onto streptavidin biosensors (ForteBio) for 120 s. After being washed in 50 mM HEPES and 150 mM NaCl (pH 7.5) for 30 s to establish baselines, 50–200 nM Fabs were associated with cdMMP-14-loaded biosensors for 120 s and then dissociated into 50 mM HEPES and 150 mM NaCl (pH 7.5) for 120 s. Averages of measured association constant k_{on} and dissociation constant k_{off} values were determined for K_D calculations.

Direct and Competitive ELISA.

Microtiter plates were coated with 5 μg/mL streptavidin and blocked with 0.5% gelatin in assay buffer [50 mM Tris-HCl (pH 7.5), 150 mM NaCl, 5 mM $CaCl_2$, and 100 μM $ZnCl_2$]. In a direct ELISA, 5 μg/mL biotinylated cdMMP-14 wt in assay buffer was added to streptavidin-coated wells for a 20 min incubation. Purified Fab was serially diluted to 1–1000 nM and incubated with immobilized cdMMP-14 at ambient temperature for 1 h. Bound Fabs were detected with an anti-Fab-HRP conjugate, and signals were developed with a TMB substrate (Thermo Fisher). The half-maximal effective concentration (EC_{50}) was calculated from a four-parameter logistic curve-fitting analysis and set as the subsaturating concentration for each tested Fab. In a competitive ELISA over cdMMP-14 mutants, Fabs at their subsaturating concentrations (e.g., 10 nM Fab 3A2) were first incubated with 0–2000 nM cdMMP-14 mutants for 2 h and then transferred to streptavidin wells coated with biotinylated cdMMP-14 wt for a 15 min incubation. Captured Fabs were measured by using an anti-Fab-HRP and a TMB substrate. For all Fab and cdMMP-14 mutant combinations, IC_{50} values were determined and Gibbs free energy changes on binding were calculated using eq 1

$$\Delta\Delta G = RT \ln \frac{IC_{50}(\text{Ala mutant})}{IC_{50}(\text{wild type})} \quad (1)$$

where $R = 1.987$ cal mol^{-1} K^{-1} and $T = 298$ K. In a competitive ELISA with nTIMP-2 or GM6001, serially diluted nTIMP-2 or GM6001 at 3 nM to 3 μM was mixed with fixed subsaturating concentrations of Fabs and incubated with biotinylated cdMMP-14 wt immobilized in streptavidin-coated wells, and bound Fabs were detected.

MMP-14 Enzymatic and Inhibition Assays.

Activities of cdMMP-14 wt and mutants were measured at 37 °C by monitoring the hydrolysis of fluorogenic peptide Mca-Lys-Pro-Leu-Gly-Leu-Dap(Dnp)-Ala-Arg-NH_2 (M-2350, Bachem) using a fluorescence microplate reader Synergy H4 (BioTek). Typically, 1 μM M-2350 was added to 30 nM cdMMP-14 in assay buffer and the initial slopes of fluorescence signals with an excitation wavelength at 328 nm and an emission wavelength at 393 nm were measured for kinetic calculation. In inhibition assays, 0–1 μM Fabs were incubated with 30 nM cdMMP-14 in assay buffer for 1 h at 37 °C, and then the reaction was initiated by adding 1 μM M-2350. The fluorescence was recorded continuously for 30 min, and the initial reaction rates and inhibition constants were calculated by fitting the data to eq 2

$$\frac{V_i}{V_o}(\%) = \frac{1}{1 + \frac{[I]}{IC_{50}}} \times 100 \quad (2)$$

where V_i is the initial velocity in the presence of the inhibitor, V_o is the initial velocity in the absence of the inhibitor, and [I] is the inhibitor concentration. To determine the type of inhibition, the initial velocity of cdMMP-14 wt as a function of substrate concentration (1–40 μM) was measured in the presence of concentrations of Fab (125–5500 nM). The values of apparent K_m and V_{max} were derived by linearization according to the Lineweaver–Burk equation.

Proteolytic Stability Test.

Purified Fabs (2 μM) were incubated with 2 μM cdMMP-14 wt in 50 mM HEPES and 150 mM NaCl (pH 7.5) at 37 °C for 4 h. Samples were analyzed by using 12% nonreducing SDS–PAGE and stained with Coomassie blue. Densitometric interpretation was conducted using a ChemiDoc imager (Bio-Rad).

RESULTS

Long CDR-H3 Potent Fabs Exhibited Competitive Inhibition.

Inspired by camelid repertoires, synthetic human antibody libraries carrying convex paratopes encoded by CDR-H3 of 23, 25, or 27 amino acids were constructed and applied for the isolation of Fabs inhibiting the catalytic domain (cd) of MMP-14.[33] To understand their inhibition mechanisms, five representative Fabs of different potencies and/or postselection abundancies were chosen in this study.[52] Four of them have CDR-H3s of 27

amino acids, and Fab 3E9 has a 25-amino acid CDR-H3 (Table 1). These Fabs also have distinct light chains especially on their CDR-L3 sequences. Fabs were produced from *E. coli* periplasm with typical yields of 0.5–2 mg of purified Fabs per liter of culture (Figure S1). Dissociation constants (K_D) measured by biolayer interferometry indicated that Fabs 3E2, 3D9, 2B5, and 3E9 exhibited affinities of 18–45 nM for cdMMP-14, while Fab 3A2 was the most efficient binder with a K_D of 7.5 nM (Figure S2). Fab 3A2 also gave a high inhibitory potency (K_I) of 8.7 nM, and Fabs 3E2, 3D9, and 2B5 had K_I values of 38–220 nM.[33] Interestingly, as a highly enriched clone after phage panning, Fab 3E9 displayed only weak inhibition with a K_I of 5.4 μM.[33] A potent inhibitory Fab DX-2400 (K_D = 1.9 nM; K_I = 4.3 nM) carrying a short CDR-H3 was characterized in this study, as well.[23,53] To determine their inhibition types (except 3E9 due to its weak potency), we measured cdMMP-14 proteolytic kinetics with a FRET peptide substrate in the presence of inhibitory Fabs at varied concentrations. The results clearly showed that for potent inhibitors 3A2, 3E2, and DX-2400, cdMMP-14 showed an unchanged maximum velocity (V_{max}) and an increased Michaelis constant (K_m) with an increasing concentration of Fabs, indicating that these Fabs inhibited cdMMP-14 proteolytic activity in a substrate competitive manner (Figure 1). For Fabs 2B5 and 3D9 of moderate potency (K_I = 220 and 55 nM, respectively), the kinetics of cdMMP-14 represented decreases in both V_{max} and K_m values, with unparallel Lineweaver–Burk plots suggesting a mixed inhibition type; i.e., 2B5 and 3D9 interfered with both cdMMP-14 as a competitive inhibitor and a cdMMP14–substrate complex as an uncompetitive inhibitor. Overall, from the synthetic human antibody libraries carrying extended CDR-H3s, all isolated Fabs exhibited at least partially competitive inhibition models, and the highly potent Fabs were exclusively competitive inhibitors (Table 1).

Inhibitory Fabs Competed with nTIMP for Binding.

The reaction center of MMP-14 and the flanking subsites form a cleftlike structure on the protease surface, which accommodates polypeptide substrates for proteolysis (Figure S3). As endogenous inhibitors of MMPs, tissue inhibitors of metalloproteinases (TIMPs) accomplish their inhibitory activities by directly binding at the active-site clefts and vicinities,[36] and thus, their competitive ELISA with antibodies can provide perceptions of antibody's binding sites. Competitive ELISAs in which each Fab at a fixed subsaturating concentration was mixed with increased amounts of nTIMP-2 were conducted, and the Fabs captured on immobilized cdMMP-14 were detected by anti-Fab-HRP for signal development. The results showed that increasing concentrations of nTIMP-2 reduced the level of binding of all six tested Fabs on immobilized cdMMP-14 (Figure 2), implying that overlaps existed between the epitopes of these Fabs and that of nTIMP-2. Notably, 3A2 displayed a sharp sigmoid curve responding to nTIMP-2, suggesting significant interference of nTIMP-2 on 3A2's binding to cdMMP-14. As nTIMP-2 makes contacts with numerous residues on surface loops surrounding the active site of MMP-14 (Figure S4),[36] some of these residue positions were considered for alanine substitutions in the following epitope mapping. In addition, results of a similar competitive ELISA with a broad spectrum reversible hydroxamate inhibitor GM6001 indicated that the bindings of all tested Fabs on cdMMP-14 were not affected by this potent inhibitor even at high concentrations of ≤3 μM (Figure S5), indicating that the MMP-14 active site is accessible for GM6001 in the presence of Fabs presumably because Fabs did not intimately contact the catalytic center.

Design and Preparation of cdMMP-14 Alanine Mutations.

To identify the binding epitopes of inhibitory Fabs, site-directed mutagenesis to alanine was used to footprint on the surface of cdMMP-14 (Figure 3). The positions for alanine scanning were selected on the basis of the cdMMP-14 structure. Considerations are (i) on the surface loops flanking its active cleft, (ii) within 15 Å of the catalytic Zn^{2+}, (iii) exhibiting an exposed respective side chain, (iv) overlapped with an epitope of nTIMP-2 (Figure S4), and (v) unique to membrane-type (MT) MMPs but not found in soluble MMPs. In particular, the 200s and 230s loops are located at the nonprime and prime sides of catalytic center, respectively. Loop 260s forms the south rim of the active cleft at the prime side, while loop 190s is at the north rim across both nonprime and prime subsites. Three positions in the MT loop (160s), displaying a high degree of sequence divergence among MMPs, were also selected for Ala substitution. A total of 20 single-point alanine mutants of cdMMP-14 were cloned and expressed in the periplasmic space of *E. coli* with yields of 60 μg to 5.1 mg of purified proteins per liter of culture (Figure S6). Notably, mutations around the active cleft led to a significantly reduced, albeit still substantial, specific activity of 0.4–8.6% relative to cdMMP-14 wt. Unsurprisingly, these mutations away from the reaction center, e.g., Y166A and E169A, or at far end of the nonprime subsites, e.g., S189A and I209A, did not drastically affect the activity. Prepared in their soluble and active form without refolding, these alanine mutants of cdMMP-14 facilitated epitope mapping with isolated antibodies.

Quantitative Mapping of Inhibitory Fab Epitopes.

At their predetermined subsaturating concentrations, Fabs bound to immobilized cdMMP-14 wt were measured in the presence of increasing amounts of cdMMP-14 alanine mutants. Such competitive ELISAs were also performed with soluble cdMMP-14 wt to obtain $IC_{50(wt)}$ values for each Fab. Compared to $IC_{50(wt)}$, the sigmoid curves associated with cdMMP-14 alanine mutants exhibited four scenarios (Figure 4): (a) abolished, e.g., Fab 3A2 completely abandoned its binding to mutant F260A; (b) weakened, e.g., Fab 3E2 showed a decreased affinity for F198A compared to cdMMP-14 wt; (c) unchanged, e.g., Fab DX-2400 had similar binding profiles with respect to D252A and wt; and (d) enhanced, e.g., Fab 3E9 bound actually better with V236A than wt. Like the additional exemplary results shown in Figure S7, 120 total competitive ELISAs for all of the combinations of 6 Fabs with 20 cdMMP-14 alanine mutants were performed for the associated $IC_{50(mut)}$ determination (Figure 5). For a direct comparison disregarding the disparity of the absolute affinity between Fabs, the effect of each alanine substitution was calculated as a change in Gibbs free energy of binding relative to that of wt: $\Delta\Delta G_{(mut-wt)} = \Delta G_{(mut)} - \Delta G_{(wt)} = RT \ln[IC_{50(mut)}/IC_{50(wt)}]$.[54] Specifically, a significant positive value of $\Delta\Delta G_{(mut-wt)}$, i.e., >0.5 kcal/mol, indicates a disruptive alanine substitution that leads to a reduced binding strength, while a significant negative $\Delta\Delta G_{(mut-wt)}$ value, i.e., less than −0.5 kcal/mol, indicates that the associated alanine substitution in fact enhances the binding strength. When the absolute value $|\Delta\Delta G_{(mut-wt)}|$ is <0.5 kcal/mol, equivalent to a <2.3-fold difference in IC_{50}, the change is considered as nonsignificant. Among all tested alanine substitutions, the most disruptive ones were at the 190s and 260s loops, e.g., F260 for 3A2, F198 and P259 for 3E2, and F260 for 3E9, with their associated $\Delta\Delta G_{(mut-wt)}$ values being >2.0 kcal/mol (corresponding to >28-fold increases in IC_{50}), suggesting that the side chains of these residues significantly contributed to binding. In addition, all Fabs except 3E9 exhibited moderate interactions with

D193 and E195 on the 190s loop with $\Delta\Delta G_{(mut-wt)}$ values of 0.5–2.0 kcal/mol (Figure 5). Interactions with these acidic residues can be possibly mediated with the basic residues in CDR-H3s of tested Fabs (Table 1). Notably, for inhibitory Fabs with high potencies (like 3A2, 3E2, and DX-2400), alanine substitutions mainly resulted in reduced affinities [positive $\Delta\Delta G_{(mut-wt)}$ values]. In contrast, for low-potency Fabs 2B5 and 3E9, many alanine substitutions gave negative energy changes, e.g., 9 of the 10 significant $\Delta\Delta G_{(mut-wt)}$ of 3E9 were less than −0.5 kcal/mol, indicating these alanine mutations improved the associated bindings.

Residues Surrounding the Active Cleft at the Prime Side Were Important Epitopes.

3A2.—Visualization of alanine scanning data on the cdMMP-14 structure suggested that 3A2 made strong contacts with residues on the 190s and 260s loops in the vicinity of the active site (Figure 6). Interactions of 3A2 with D193, E195, and Y261 side chains accounted for a binding energy of 1.2–1.8 kcal/mol each, corresponding to 7.5–21-fold decreases in affinity when these residues were mutated to alanine. The strongest interaction between 3A2 and cdMMP-14 was mediated by F260, because alanine mutation at this position eliminated binding activity completely (Figure 4A). Weak interactions also occurred with the side chains of E169, N229, and S250, with decreases in the free energy of binding of 0.6–0.8 kcal/mol. Notably, residues that strongly interact with 3A2 are all located at the prime side of the cdMMP-14 active center on the north and south rims of the reaction cleft. In contrast, alanine substitutions at the nonprime side of cdMMP-14, including Y203, F204, and I209 on the 200s loop and S189 and T190 on the 190s loop, did not cause significant changes in $\Delta\Delta G_{(mut-wt)}$, suggesting these residues made little contribution to 3A2's recognition. In addition, alanine mutations at N231 and V236, which lie in the bottom of the catalytic cleft, also did not affect the binding affinity, suggesting that Fab 3A2 did not tightly contact with the cleft bottom of cdMMP-14, consistent with the results of the competitive ELISA with GM6001 (Figure S5). Overall, 3A2 recognizes the prime side surface loops of cdMMP-14 in the vicinity of its active cleft.

3E2.—Epitope mapping with Fab 3E2 also demonstrated the importance of the prime side (Figure 6). 3E2 exhibited strong interactions with F198 and P259; both are close to the S1′ subsite located on the north and south rims, respectively. Their alanine substitutions increased the IC_{50} values to >0.9 μM, corresponding to substantial changes in binding energy of >2.4 kcal/mol (Figure 5). In addition, alanine mutations of numerous prime side residues, including D193 and E195 on the 190s loop, N229 and V236 on the 230s loop, and F260 and Y261 on the 260s loop, all had significant effects on 3E2 binding (0.5–2.0 kcal/mol each). In contrast, S189 and the 200s loop, located at the nonprime side, had no significant contributions. Different from 3A2, 3E2 also formed moderate interactions with S251 and D252 on the 250s loop (1.7 kcal/mol collectively) and a weak interaction with T190 close to the S1 subsite, indicating a large binding footprint compared to that of 3A2, though their epitopes were mainly overlapped at the prime side of the cleft rims.

2B5 and DX-2400.—These Fabs shared their epitopes on the prime side surface loops of 190s (D193 and E195 for both), 230s (229N for DX-2400 and 231N for 2B5), and 260s (F261 for both) mostly through combinations of these minor interactions (0.5–1.0 kcal/mol

each) (Figure 5). The only exception was the N231A variant that generated a moderate change in free energy on 2B5 binding (1.6 kcal/mol, equivalent to a 14-fold weakened IC_{50}). In addition, neither 2B5 nor DX-2400 made contact with nonprime side residues S189, Y203, F204, and I209 or the 250s loop (Figure 6). Notably, several alanine substitutions on cdMMP-14 improved their recognition by the Fabs, e.g., Y166, R168, and T190 for 2B5 and F198 and P259 for DX-2400. These modest decreases in binding energy (0.5–0.7 kcal/mol) suggested that interactions via the side chains of these residues were suboptimal. As a potent inhibitor with a high binding affinity of 1.9 nM, Fab DX-2400 surprisingly made only four contacts of modest strength among the tested positions, implying that an epitope other than the mapped area may exist for DX-2400.

3E9 and 3D9.—3E9 gained much of its binding energy from a strong interaction with the side chain of F260, as an alanine mutation at this position led to a 33-fold increase in IC_{50} (2.1 kcal/mol) (Figure 5). Centered at F260, low-affinity Fab 3E9 also made suboptimal contacts [negative $\Delta\Delta G_{(mut-wt)}$ values] with nine residues scattered on the 160s, 190s, 230s, 250s, and 260s loops (Figure 6). Markedly, a majority of these residues and F260 were located at the prime side related to the cdMMP-14 active site. In contrast, 3D9 formed significant interactions with the side chains of two residues, D193 (1.1 kcal/mol) at the prime side and F204 (0.7 kcal/mol) at the nonprime side (Figure 5). Notably, 3D9 also exhibited a negative $\Delta\Delta G_{(mut-wt)}$ with T190 at the prime side and weak interactions with N231 and P259 at the nonprime side (Figure 6). All of these observations made 3D9 the only exception that had epitopes across both sides of the reaction center, different from all other tested Fabs.

Contribution of 3A2 CDR-H3 to Inhibition and Stability.

The mechanism of inhibition of highly potent Fab 3A2 was further characterized by paratope alanine mutations. Previous study has suggested that although ineffective as a substrate, Fab 3A2 can be slowly cleaved by MMP-14 with the scissile peptide bond between residues N100h (P1) and L100i (P1′) within its CDR-H3 (Figure 7A).[44] Large-scale substrate profiling has identified MMP-14's subsite amino acid preference:[55] Ala at P2, Gly/Asn/Ala at P1, Leu/Ile/Val at P1′, Val/Ile/Leu at P2′, Gly/His/Ala at P3′, and Pro/Asp/Val at P5′. Remarkably, these underlined residues are well matched with the central portion of the 3A2 CDR-H3 sequence ($_{100h}$NLVATP$_{100m}$). These observations together with epitope mapping results (Figure 6) imply that this portion of CDR-H3 of 3A2 complements MMP-14 subsites S1–S5′ and thus encourage us to introduce alanine substitutions into 3A2 CDR-H3. More specifically, two positions at the C-terminus of the scissile bond, L100i and T100l, correspond to the prime substrate residues P1′ and P4′, respectively, and two residues, R100g and W100e, at the nonprime (N-terminal side of the scissile bond) P2 and P4 positions were selected for alanine mutations (shaded in Figure 7A). Notably, mutant R100gA flipped P2 from an under-represented substrate residue of MMP-14 to an over-represented one,[55] and in contrast, mutant L100iA changed the P1′ residue from MMP-14 preferred to disfavored. These four Fabs of 3A2 alanine mutants were produced (Figure S8). Biolayer interferometry indicated that 3A2 mutants R100gA(P2) and W100eA(P4) kept their binding affinities for cdMMP-14 with K_D values of 5.7 and 6.6 nM, respectively (Figure S9), similar to that of 3A2 wt. Assays with a FRET peptide substrate suggested that

these two nonprime paratope mutants also effectively retained their inhibitory potency (Figure 7B). In contrast, alanine substitutions at two prime paratope sites, L100iA and T100lA, exhibited reduced affinities with K_D values of 21 and 27 nM, respectively (Figure S9 and Figure 7B). In addition, mutant L100iA at position P1′ dramatically decreased its inhibitory potency 290-fold, and mutant T100lA at P4′, distant from the cleavage site, compromised the inhibitory function to a lesser but still significant degree with a 3.3-fold weakened K_I (Figure 7C). These results not only echoed the importance of prime subsites as binding epitopes (Figure 6) but also suggested a direct contribution of the 3A2 CDR-H3 prime portion for inhibition function. To understand the possible role of the nonprime portion of 3A2 CDR-H3, we further measured the proteolytic liability of Fabs 3A2 wt, W100eA, and R100gA. After incubation of 2 μM Fab (3A2 wt or its alanine mutants) with 2 μM cdMMP-14 for 4 h at 37 °C and pH 7.5, densitometric analysis by nonreducing SDS–PAGE revealed that compared to 3A2 wt, W100eA and R100gA resulted in significantly more truncated Fab fragments, i.e., 1.9- and 1.6-fold increases for LC-C_H1 and 3.0- and 2.0-fold increases for V_H, respectively (Figure 7D), suggesting the nonprime portion of CDR-H3 was important for proteolytic stability.

DISCUSSION

This study has identified the molecular mechanisms by which Fabs of convex paratopes, isolated from synthetic human antibody libraries carrying long CDR-H3s, inhibit proteolytic activity of MMP-14. In addition to enzyme kinetics and a competitive ELISA over physiological or synthetic inhibitors, binding landscapes have been quantitatively mapped by using series of cdMMP-14 alanine mutants. Collectively, the results indicate that these Fabs of extended H3s are competitive inhibitors recognizing the vicinity of the active cleft especially on the prime side of the active site. The most significant epitopes are scattered across the north and south rims of the cleft, i.e., 190s and 260s loops, respectively (Figure 6), but less pronounced at the bottom of the cleft. These results are consistent with observations that nTIMP-2 but not GM6001 can replace Fabs on binding to cdMMP-14 (Figure 2 and Figure S5). Indeed, Fab epitopes overlap with that of nTIMP-2 but cannot block potent GM6001 to access the active site, implying that a void may exist between Fabs and cdMMP-14 in their complexes. Nevertheless, Fab 3A2 can be inefficiently and slowly cleaved at its CDR-H3 by cdMMP-14 (Figure 7D),[44] suggesting that its H3 loop must possess a certain flexibility to be able to approach the catalytic center. Analysis of the scissile bond on Fab 3A2 and profiles of the MMP-14 substrate preference[44,55] implies that the middle part of 3A2 CDR-H3, $_{100h}$NLVATP$_{100m}$, complements MMP-14 subsites S1–S5′ (Figure 8A). Although recognized by MMP-14 in a substrate-like manner, Fab 3A2 behaves as a strong inhibitor and/or poor substrate, presumably because its interactions with cleft rims are limited primarily to one side of the catalytic zinc, unlike real substrates with intimate contacts with subsites at the bottom of the cleft on both sides. This understanding of 3A2 CDR-H3 function is further supported by paratope mutagenesis studies. Changing P1′ to an unfavorable residue, L100iA, causes the P1′ residue to detach from subsite S1′ (Figure 8B) and thus exposes the catalytic center for substrate access and dramatically decreases the inhibitory potency (Figure 7C). On the contrary, paratope mutation R100gA changes P2 to a MMP-14 preferred substrate residue and thus promotes subsite occupation at S2 and extends

the recognition covering S2–S5′ (Figure 8C). Like a substrate, R100gA binds both prime and nonprime subsites and thus is more vulnerable to cdMMP-14 cleavage than 3A2 wt (Figure 7D). Overall, Fab 3A2 is a canonical (substrate-like) inhibitor, achieving its function via direct interactions with the active-site cleft of MMP-14 by using its 27-amino acid extended CDR-H3 likely forming a convex-shaped paratope. For other Fabs of long CDR-H3s tested in this study, however, no clear substrate patterns can be identified within their CDRs.

Numerous mAbs targeting a variety of proteases have been biochemically and/or structurally elucidated. On the basis of their inhibition mechanisms, a majority of these mAbs can be classified as active-site or exosite inhibitors.[56,57] Binding to epitopes other than the catalytic center, an exosite inhibitor usually triggers conformational changes at or around the active cleft and thus interferes with access to the substrate.[21,25,58] Interestingly, such allosteric effects are also feasible for accelerating proteolytic reactions for certain substrates.[59,60] In contrast, an active-site inhibitor forms intimate contacts with the protease reaction center that is located in the middle of the active cleft.[35,56] To reach the reaction pockets, prolate structures are often observed among the paratopes of active-site inhibitors.[35] Isolated from synthetic libraries, anti-matriptase mAbs E2, A11, and S4[22,27] and anti-pKal DX-2930[28] all carry extended length CDR-H3s that form protruded conformations to insert into the protease active sites. On the contrary, anti-FXIa DEF[61] and anti-MMP9 SDS3,[24] isolated from naïve and immunized libraries, respectively, have short H3s but intriguingly use their L1 or H2 on the edge of their overall concave paratopes for active-site penetration. Alternatively, substrate access can be blocked without intimate contacts at the active site, as demonstrated by anti-HGFA Ab58, for instance.[21] In this study, inhibitory Fabs of long H3s exhibit their main epitopes in the vicinity of the active cleft; e.g., 3E2 strongly interacts with subsite S1′, and 3D9 has epitopes across both prime and nonprime sides of the cleft (Figures 5 and 6). Considering their 25- or 27-amino acid extended CDR-H3s, convex paratopes are probably formed for direct interactions with the active cleft. However, these interpretations can be confirmed only by determining the structures of the Fab–cdMMP-14 complex.

Various strategies for decreasing the proteolytic liability have been exploited by active-site inhibitors: (i) a cleavage–resynthesis equilibrium, e.g., bovine pancreatic trypsin inhibitor,[62] (ii) reverse orientation of inserted loops, e.g., anti-matriptase A11 and S4,[27] and anti-FXIa DEF,[61] and (iii) occupation of one but not both sides of the catalytic center, e.g., anti-pKal DX-2930.[28] More specifically, CDR-H3 of DX-2930 binds S1–S3 and abruptly turns away from the prime subsites, thereby preventing cleavage by the catalytic serine of pKal. In contrast, camelid anti-uPA Nb4 inserts its CDR-H3 into the entire S4–S3′ substrate-binding pocket, leading to substantial proteolytic cleavage.[63] This study indicates that most tested Fabs of MMP-14 inhibition dominate their recognition on the prime side of the cleft (Figure 6). In addition, binding of Fab 3A2 to cdMMP-14 is unaffected even with high concentrations of GM6001 (Figure S5), implying an unintimate contact between its H3 and the catalytic site. Presumably, the two reasons mentioned above cause Fab 3A2 to be an inefficient substrate. Paratope mutagenesis supports this notion as extending subsite occupation to S2 makes Fab 3A2 mutant R100gA more sensitive to proteolysis (Figure 7D). On the contrary, converting P1 and/or P3′ to MMP-14 unfavored residues significantly improves the stability without compromising the inhibitory potency.[44] In addition to

proteolytic stability, specificity is another required property for protease inhibition-based therapies. The catalytic domains of MMP family members share a homologous protein folding and secondary structures.[64] Despite their highly conserved catalytic Zn^{2+} and associated motifs, sequential and conformational diversity does exist among MMPs, especially at their surface loops surrounding the active cleft to determine their substrate specificity.[65] This study indicates that these surface loops are important epitopes for all tested Fab inhibitors (Figure 6), explaining at least partially why these Fabs are highly selective as reported previously.[33]

Because of their pivotal roles in extracellular matrix remodeling, MMPs have been regarded as one of the most important regulatory enzymes for a variety of conditions (e.g., tumor invasion and metastasis, development of obesity, and neuropathy),[41–43] and thus striking therapeutic targets for associated treatments.[66,67] Isolated from synthetic libraries carrying convex paratopes, MMP inhibitory mAbs have demonstrated significant therapeutic efficacies in mouse models. (i) Fab 3A2 reduced both the frequency and the size of melanoma metastatic nodules.[40] (ii) IgG 3A2 markedly inhibited growth of the primary breast tumor and more importantly reduced the metastatic spread to the lungs and liver by >90%.[41] (iii) Treatment with IgG 3A2 improved glucose intolerance and decreased the body weight in both mice with obesity induced by a high-fat diet and *ob/ob* mice (unpublished). (iv) Anti-MMP-9 IgG L13 exhibited neuropathic pain attenuation efficacy in chemotherapy-induced pain[34] and diabetic neuropathy (unpublished). In addition, pharmacokinetic analysis further suggested that IgG 3A2 had an *in vivo* half-life of ~4.8 days,[41] similar to that of serum IgGs in adult mice.

CONCLUSIONS

In this study, MMP-14 inhibitory Fabs carrying 25- or 27-amino acid CDR-H3s have been biochemically characterized. The results indicate that these Fabs recognize the highly diverse region among MMPs and dominantly target the prime side of the active cleft and its vicinity. The canonical (substrate-like) mechanism of Fab 3A2 and the exact contribution of its CDR-H3 to inhibition have also been revealed. These findings suggest the underlying principles for selectivity and proteolytic resistance of these Fabs. Understanding the molecular mechanism and previous preclinical results mutually support the idea that synthetic antibody libraries encoding extended CDR-H3s are a valuable resource, from which isolated human mAbs hold great therapeutic promise to effectively and selectively inhibit biomedically important proteases.

Supplementary Material

Refer to Web version on PubMed Central for supplementary material.

ACKNOWLEDGMENTS

The authors are thankful for UCR Graduate Division’s Dissertation Year Program (DYP) Awards to D.H.N. and K.B.L. and the Mogam Science Scholarship Foundation Fellowship to K.B.L.

Funding

This work was supported by National Institutes of Health Grant 1R01GM115672 and National Science Foundation CAREER Grant 1453645.

REFERENCES

(1). Turk B, Turk D, and Turk V (2012) Protease signalling: the cutting edge. EMBO J. 31, 1630–1643. [PubMed: 22367392]

(2). López-Otín C, and Bond JS (2008) Proteases: multifunctional enzymes in life and disease. J. Biol. Chem 283, 30433–30437. [PubMed: 18650443]

(3). Deu E, Verdoes M, and Bogyo M (2012) New approaches for dissecting protease functions to improve probe development and drug discovery. Nat. Struct. Mol. Biol 19, 9–16. [PubMed: 22218294]

(4). Docherty AJ, Crabbe T, O'Connell JP, and Groom CR (2003) Proteases as drug targets. Biochem. Soc. Symp 70, 147–161.

(5). Prassas I, Eissa A, Poda G, and Diamandis EP (2015) Unleashing the therapeutic potential of human kallikrein-related serine proteases. Nat. Rev. Drug Discovery 14, 183–202. [PubMed: 25698643]

(6). Singh RB, Dandekar SP, Elimban V, Gupta SK, and Dhalla NS (2004) Role of proteases in the pathophysiology of cardiac disease. Mol. Cell. Biochem 263, 241–256.

(7). López-Otín C, and Matrisian LM (2007) Emerging roles of proteases in tumour suppression. Nat. Rev. Cancer 7, 800–808. [PubMed: 17851543]

(8). Ji RR, Xu ZZ, Wang X, and Lo EH (2009) Matrix metalloprotease regulation of neuropathic pain. Trends Pharmacol. Sci 30, 336–340. [PubMed: 19523695]

(9). De Strooper B (2010) Proteases and proteolysis in Alzheimer disease: a multifactorial view on the disease process. Physiol. Rev 90, 465–494. [PubMed: 20393191]

(10). Troeberg L, and Nagase H (2012) Proteases involved in cartilage matrix degradation in osteoarthritis. Biochim. Biophys. Acta, Proteins Proteomics 1824, 133–145.

(11). Greenbaum DC, Baruch A, Grainger M, Bozdech Z, Medzihradszky KF, Engel J, DeRisi J, Holder AA, and Bogyo M (2002) A role for the protease falcipain 1 in host cell invasion by the human malaria parasite. Science (Washington, DC, U. S.) 298, 2002–2006.

(12). Lorenz IC, Marcotrigiano J, Dentzer TG, and Rice CM (2006) Structure of the catalytic domain of the hepatitis C virus NS2–3 protease. Nature 442, 831–835. [PubMed: 16862121]

(13). Wensing AM, van Maarseveen NM, and Nijhuis M (2010) Fifteen years of HIV Protease Inhibitors: raising the barrier to resistance. Antiviral Res. 85, 59–74. [PubMed: 19853627]

(14). Böttcher E, Matrosovich T, Beyerle M, Klenk HD, Garten W, and Matrosovich M (2006) Proteolytic activation of influenza viruses by serine proteases TMPRSS2 and HAT from human airway epithelium. J. Virol 80, 9896–9898. [PubMed: 16973594]

(15). Drag M, and Salvesen GS (2010) Emerging principles in protease-based drug discovery. Nat. Rev. Drug Discovery 9, 690–701. [PubMed: 20811381]

(16). Puente XS, Sánchez LM, Overall CM, and López-Otín C (2003) Human and mouse proteases: a comparative genomic approach. Nat. Rev. Genet 4, 544–558. [PubMed: 12838346]

(17). Tallant C, Marrero A, and Gomis-Rüth FX (2010) Matrix metalloproteinases: fold and function of their catalytic domains. Biochim. Biophys. Acta, Mol. Cell Res 1803, 20–28.

(18). Overall CM, and Kleifeld O (2006) Towards third generation matrix metalloproteinase inhibitors for cancer therapy. Br. J. Cancer 94, 941–946. [PubMed: 16538215]

(19). Kessenbrock K, Plaks V, and Werb Z (2010) Matrix metalloproteinases: regulators of the tumor microenvironment. Cell 141, 52–67. [PubMed: 20371345]

(20). Zucker S, and Cao J (2009) Selective matrix metalloproteinase (MMP) inhibitors in cancer therapy: ready for prime time? Cancer Biol. Ther 8, 2371–2373. [PubMed: 19959934]

(21). Wu Y, Eigenbrot C, Liang WC, Stawicki S, Shia S, Fan B, Ganesan R, Lipari MT, and Kirchhofer D (2007) Structural insight into distinct mechanisms of protease inhibition by antibodies. Proc. Natl. Acad. Sci. U. S. A 104, 19784–19789. [PubMed: 18077410]

(22). Farady CJ, Egea PF, Schneider EL, Darragh MR, and Craik CS (2008) Structure of an Fab-protease complex reveals a highly specific non-canonical mechanism of inhibition. J. Mol. Biol 380, 351–360. [PubMed: 18514224]

(23). Devy L, Huang L, Naa L, Yanamandra N, Pieters H, Frans N, Chang E, Tao Q, Vanhove M, Lejeune A, van Gool R, Sexton DJ, Kuang G, Rank D, Hogan S, Pazmany C, Ma YL, Schoonbroodt S, Nixon AE, Ladner RC, Hoet R, Henderikx P, Tenhoor C, Rabbani SA, Valentino ML, Wood CR, and Dransfield DT (2009) Selective inhibition of matrix metalloproteinase-14 blocks tumor growth, invasion, and angiogenesis. Cancer Res. 69, 1517–1526. [PubMed: 19208838]

(24). Sela-Passwell N, Kikkeri R, Dym O, Rozenberg H, Margalit R, Arad-Yellin R, Eisenstein M, Brenner O, Shoham T, Danon T, Shanzer A, and Sagi I (2012) Antibodies targeting the catalytic zinc complex of activated matrix metalloproteinases show therapeutic potential. Nat. Med 18, 143–147.

(25). Atwal JK, Chen Y, Chiu C, Mortensen DL, Meilandt WJ, Liu Y, Heise CE, Hoyte K, Luk W, Lu Y, Peng K, Wu P, Rouge L, Zhang Y, Lazarus RA, Scearce-Levie K, Wang W, Wu Y, Tessier-Lavigne M, and Watts RJ (2011) A therapeutic antibody targeting BACE1 inhibits amyloid-β production in vivo. Sci. Transl. Med 3, 84ra43.

(26). Naito S, Takahashi T, Onoda J, Yamauchi A, Kawai T, Kishino J, Yamane S, Fujii I, Fukui N, and Numata Y (2012) Development of a neutralizing antibody specific for the active form of matrix metalloproteinase-13. Biochemistry 51, 8877–8884. [PubMed: 23050690]

(27). Schneider EL, Lee MS, Baharuddin A, Goetz DH, Farady CJ, Ward M, Wang CI, and Craik CS (2012) A reverse binding motif that contributes to specific protease inhibition by antibodies. J. Mol. Biol 415, 699–715. [PubMed: 22154938]

(28). Kenniston JA, Faucette RR, Martik D, Comeau SR, Lindberg AP, Kopacz KJ, Conley GP, Chen J, Viswanathan M, Kastrapeli N, Cosic J, Mason S, DiLeo M, Abendroth J, Kuzmic P, Ladner RC, Edwards TE, TenHoor C, Adelman BA, Nixon AE, and Sexton DJ (2014) Inhibition of plasma kallikrein by a highly specific active site blocking antibody. J. Biol. Chem 289, 23596–23608. [PubMed: 24970892]

(29). Appleby TC, Greenstein AE, Hung M, Liclican A, Velasquez M, Villaseñor AG, Wang R, Wong MH, Liu X, Papalia GA, Schultz BE, Sakowicz R, Smith V, and Kwon HJ (2017) Biochemical characterization and structure determination of a potent, selective antibody inhibitor of human MMP9. J. Biol. Chem 292, 6810–6820. [PubMed: 28235803]

(30). David T, Kim YC, Ely LK, Rondon I, Gao H, O'Brien P, Bolt MW, Coyle AJ, Garcia JL, Flounders EA, Mikita T, and Coughlin SR (2016) Factor XIa-specific IgG and a reversal agent to probe factor XI function in thrombosis and hemostasis. Sci. Transl. Med 8, 353ra112.

(31). Ling B, Watt K, Banerjee S, Newsted D, Truesdell P, Adams J, Sidhu SS, and Craig AWB (2017) A novel immunotherapy targeting MMP-14 limits hypoxia, immune suppression and metastasis in triple-negative breast cancer models. Oncotarget 8, 58372–58385. [PubMed: 28938563]

(32). Razai AS, Eckelman BP, and Salvesen GS (2020) Selective inhibition of matrix metalloproteinase 10 (MMP10) with a single-domain antibody. J. Biol. Chem 295, 2464–2472. [PubMed: 31953328]

(33). Nam DH, Rodriguez C, Remacle AG, Strongin AY, and Ge X (2016) Active-site MMP-selective antibody inhibitors discovered from convex paratope synthetic libraries. Proc. Natl. Acad. Sci. U. S. A 113, 14970–14975. [PubMed: 27965386]

(34). Lopez T, Mustafa Z, Chen C, Lee KB, Ramirez A, Benitez C, Luo X, Ji RR, and Ge X (2019) Functional selection of protease inhibitory antibodies. Proc. Natl. Acad. Sci. U. S. A 116, 16314–16319. [PubMed: 31363054]

(35). Farady CJ, and Craik CS (2010) Mechanisms of macromolecular protease inhibitors. ChemBioChem 11, 2341–2346. [PubMed: 21053238]

(36). Fernandez-Catalan C, Bode W, Huber R, Turk D, Calvete JJ, Lichte A, Tschesche H, and Maskos K (1998) Crystal structure of the complex formed by the membrane type 1-matrix metalloproteinase with the tissue inhibitor of metalloproteinases-2, the soluble progelatinase A receptor. Embo j 17, 5238–5248. [PubMed: 9724659]

(37). Lauwereys M, Arbabi Ghahroudi M, Desmyter A, Kinne J, Hölzer W, De Genst E, Wyns L, and Muyldermans S (1998) Potent enzyme inhibitors derived from dromedary heavy-chain antibodies. Embo j 17, 3512–3520. [PubMed: 9649422]

(38). Desmyter A, Transue TR, Ghahroudi MA, Dao Thi MH, Poortmans F, Hamers R, Muyldermans S, and Wyns L (1996) Crystal structure of a camel single-domain VH antibody fragment in complex with lysozyme. Nat. Struct. Mol. Biol 3, 803–811.

(39). De Genst E, Silence K, Decanniere K, Conrath K, Loris R, Kinne J, Muyldermans S, and Wyns L (2006) Molecular basis for the preferential cleft recognition by dromedary heavy-chain antibodies. Proc. Natl. Acad. Sci. U. S. A 103, 4586–4591. [PubMed: 16537393]

(40). Remacle AG, Cieplak P, Nam DH, Shiryaev SA, Ge X, and Strongin AY (2017) Selective function-blocking monoclonal human antibody highlights the important role of membrane type-1 matrix metalloproteinase (MT1-MMP) in metastasis. Oncotarget 8, 2781–2799. [PubMed: 27835863]

(41). Chen KE, Chen C, Lopez T, Radecki KC, Bustamante K, Lorenson MY, Ge X, and Walker AM (2018) Use of a novel camelid-inspired human antibody demonstrates the importance of MMP-14 to cancer stem cell function in the metastatic process. Oncotarget 9, 29431–29444. [PubMed: 30034628]

(42). Ji RR, Xu ZZ, Wang X, and Lo EH (2009) Matrix metalloprotease regulation of neuropathic pain. Trends Pharmacol. Sci 30, 336–340. [PubMed: 19523695]

(43). Li X, Zhao Y, Chen C, Yang L, Lee HH, Wang Z, Zhang N, Kolonin MG, An Z, Ge X, Scherer PE, and Sun K (2020) Critical Role of Matrix Metalloproteinase 14 in Adipose Tissue Remodeling during Obesity. Mol. Cell. Biol 40, No. e00564–19. [PubMed: 31988105]

(44). Lee KB, Dunn Z, and Ge X (2019) Reducing proteolytic liability of a MMP-14 inhibitory antibody by site-saturation mutagenesis. Protein Sci. 28, 643–653. [PubMed: 30592555]

(45). Lopez T, Ramirez A, Benitez C, Mustafa Z, Pham H, Sanchez R, and Ge X (2018) Selectivity Conversion of Protease Inhibitory Antibodies. Antibody Ther. 1, 75.

(46). Lopez T, Chuan C, Ramirez A, Chen KE, Lorenson MY, Benitez C, Mustafa Z, Pham H, Sanchez R, Walker AM, and Ge X (2018) Epitope-specific affinity maturation improved stability of potent protease inhibitory antibodies. Biotechnol. Bioeng 115, 2673–2682. [PubMed: 30102763]

(47). Hayhurst A, Happe S, Mabry R, Koch Z, Iverson BL, and Georgiou G (2003) Isolation and expression of recombinant antibody fragments to the biological warfare pathogen Brucella melitensis. J. Immunol. Methods 276, 185–196. [PubMed: 12738372]

(48). Nam DH, and Ge X (2016) Direct production of functional matrix metalloproteinase–14 without refolding or activation and its application for in vitro inhibition assays. Biotechnol. Bioeng 113, 717–723. [PubMed: 26416249]

(49). Nam DH, Lee KB, and Ge X (2018) Functional Production of Catalytic Domains of Human MMPs in Escherichia coli Periplasm. Methods Mol. Biol. (N. Y., NY, U. S.) 1731, 65–72.

(50). Nam DH, and Ge X (2018) Generation of Highly Selective MMP Antibody Inhibitors. Methods Mol. Biol. (N. Y., NY, U. S.) 1731, 307–324.

(51). Lee KB, Nam DH, Nuhn JAM, Wang J, Schneider IC, and Ge X (2017) Direct expression of active human tissue inhibitors of metalloproteinases by periplasmic secretion in Escherichia coli. Microb. Cell Fact 16, 73. [PubMed: 28454584]

(52). Lopez T, Nam DH, Kaihara E, Mustafa Z, and Ge X (2017) Identification of highly selective MMP-14 inhibitory Fabs by deep sequencing. Biotechnol. Bioeng 114, 1140–1150. [PubMed: 28090632]

(53). Muruganandam A, Tenhoor C, and Devy L (2009) Methods and compositions comprising anti-idiotypic antibodies to anti-mmp-14 antibodies. WO 2009132251 A2.

(54). Cunningham BC, and Wells JA (1993) Comparison of a structural and a functional epitope. J. Mol. Biol 234, 554–563. [PubMed: 7504735]

(55). Eckhard U, Huesgen PF, Schilling O, Bellac CL, Butler GS, Cox JH, Dufour A, Goebeler V, Kappelhoff R, Keller UAD, Klein T, Lange PF, Marino G, Morrison CJ, Prudova A, Rodriguez D, Starr AE, Wang Y, and Overall CM (2016) Active site specificity profiling of the matrix metalloproteinase family: Proteomic identification of 4300 cleavage sites by nine MMPs

explored with structural and synthetic peptide cleavage analyses. Matrix Biol. 49, 37–60. [PubMed: 26407638]

(56). Ganesan R, Eigenbrot C, and Kirchhofer D (2010) Structural and mechanistic insight into how antibodies inhibit serine proteases. Biochem. J 430, 179–189. [PubMed: 20704569]

(57). Wang W, Liu Y, and Lazarus RA (2013) Allosteric inhibition of BACE1 by an exosite-binding antibody. Curr. Opin. Struct. Biol 23, 797–805. [PubMed: 23998983]

(58). Udi Y, Grossman M, Solomonov I, Dym O, Rozenberg H, Moreno V, Cuniasse P, Dive V, Arroyo AG, and Sagi I (2015) Inhibition mechanism of membrane metalloprotease by an exosite-swiveling conformational antibody. Structure (Oxford, U. K.) 23, 104–115.

(59). Zhou L, Chávez-Gutierréz L, Bockstael K, Sannerud R, Annaert W, May PC, Karran E, and De Strooper B (2011) Inhibition of beta-secretase in vivo via antibody binding to unique loops (D and F) of BACE1. J. Biol. Chem 286, 8677–8687. [PubMed: 21209097]

(60). Petersen HH, Hansen M, Schousboe SL, and Andreasen PA (2001) Localization of epitopes for monoclonal antibodies to urokinase-type plasminogen activator: relationship between epitope localization and effects of antibodies on molecular interactions of the enzyme. Eur. J. Biochem 268, 4430–4439. [PubMed: 11502203]

(61). Ely LK, Lolicato M, David T, Lowe K, Kim YC, Samuel D, Bessette P, Garcia JL, Mikita T, Minor DL Jr., and Coughlin SR (2018) Structural Basis for Activity and Specificity of an Anticoagulant Anti-FXIa Monoclonal Antibody and a Reversal Agent. Structure (Oxford, U. K.) 26, 187–198.

(62). Zakharova E, Horvath MP, and Goldenberg DP (2009) Structure of a serine protease poised to resynthesize a peptide bond. Proc. Natl. Acad. Sci. U. S. A 106, 11034–11039. [PubMed: 19549826]

(63). Kromann-Hansen T, Oldenburg E, Yung KW, Ghassabeh GH, Muyldermans S, Declerck PJ, Huang M, Andreasen PA, and Ngo JC (2016) A Camelid-derived Antibody Fragment Targeting the Active Site of a Serine Protease Balances between Inhibitor and Substrate Behavior. J. Biol. Chem 291, 15156–15168. [PubMed: 27226628]

(64). Gomis-Rüth FX (2009) Catalytic domain architecture of metzincin metalloproteases. J. Biol. Chem 284, 15353–15357. [PubMed: 19201757]

(65). Nagase H (2001) Substrate Specificity of MMPs In Matrix Metalloproteinase Inhibitors in Cancer Therapy (Clendeninn NJ, and Appelt K, Eds.) pp 39–66, Humana Press, Totowa, NJ.

(66). Roy R, Yang J, and Moses MA (2009) Matrix metalloproteinases as novel biomarkers and potential therapeutic targets in human cancer. J. Clin. Oncol 27, 5287–5297. [PubMed: 19738110]

(67). Fingleton B (2007) Matrix metalloproteinases as valid clinical targets. Curr. Pharm. Des 13, 333–346. [PubMed: 17313364]

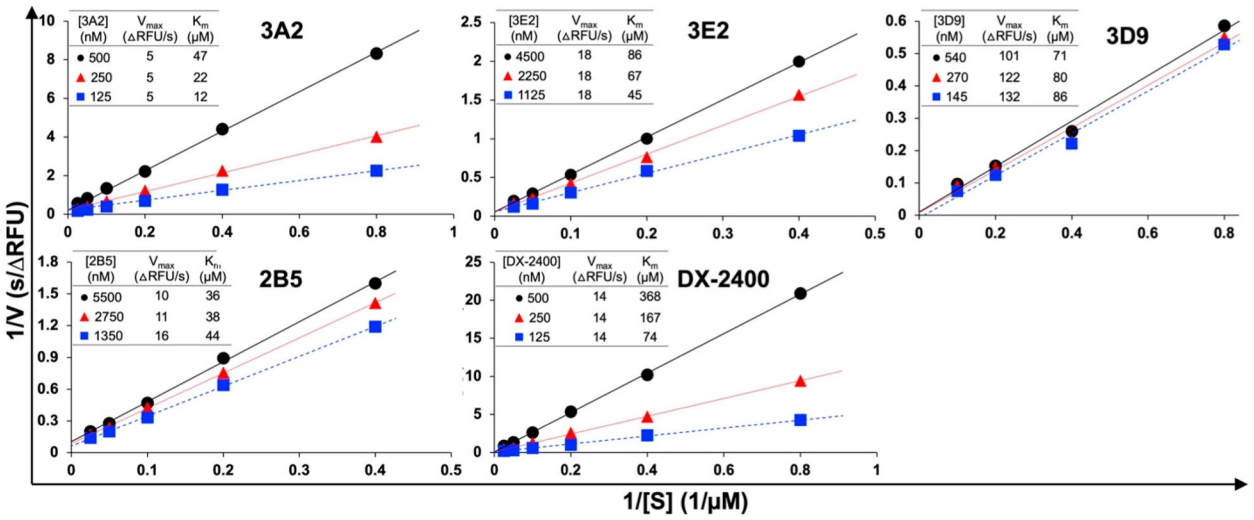

Figure 1.

Mode of inhibition determined by kinetics. Reaction rates were measured with 30 nM cdMMP-14 and 1–40 μM FRET peptide substrate M-2350 in the presence of Fabs at various concentrations. With unchanged V_{max} and increased apparent K_m values, 3A2, 3E2, and DX-2400 exhibited competitive inhibition, while 2B5 and 3D9 were mixed model inhibitors (competitive and uncompetitive).

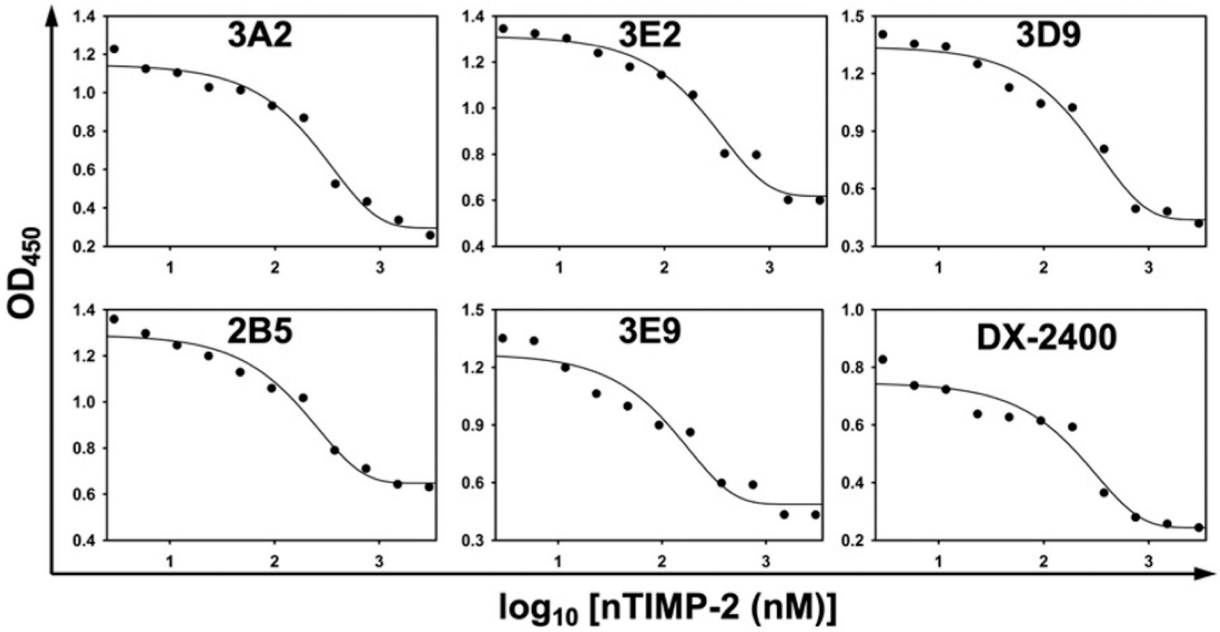

Figure 2.

Competitive ELISA with nTIMP-2. Immobilized cdMMP-14 was incubated with Fabs (3A2, 3D9, and DX-2400 at 10 nM; 3E2, 2B5, and 3E9 at 20 nM) in the presence of 3 nM to 3 μM nTIMP-2. Anti-Fab-HRP was used to detect the captured Fabs.

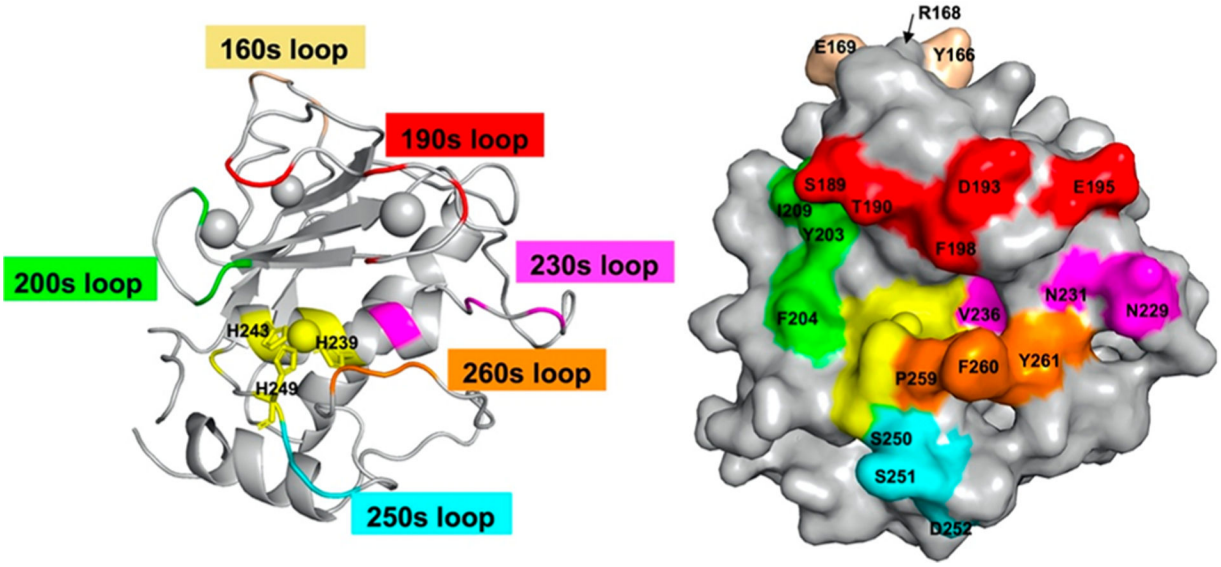

Figure 3.

Design of cdMMP-14 alanine point mutants. Structures of cdMMP-14 displayed as a cartoon (left) and in a surface mode (right) show the loops and residues selected for alanine point mutations. The catalytic zinc and its coordinating histidines (sticks) are colored yellow.

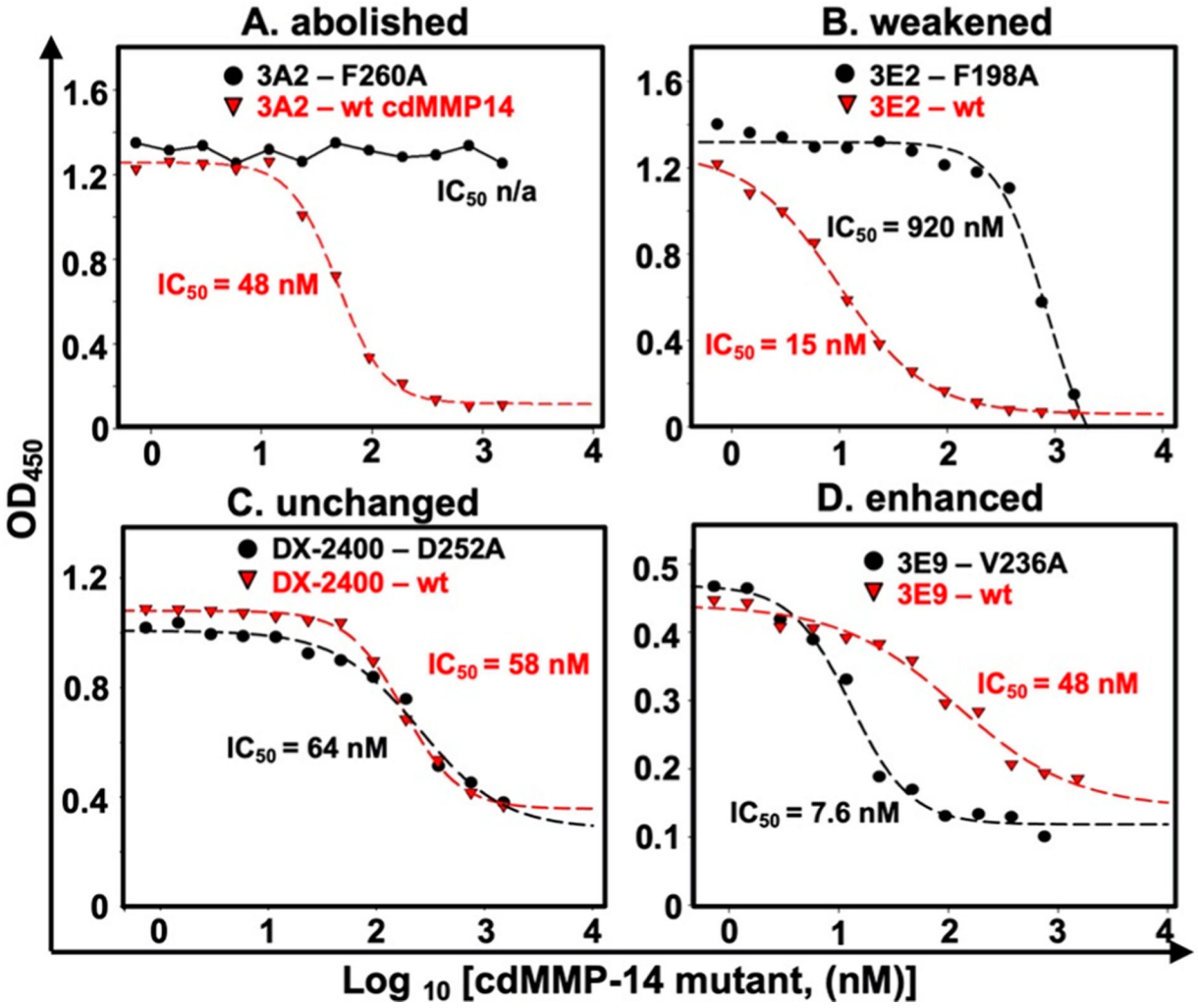

Figure 4.

Exemplary results of a competitive ELISA with wt and alanine-substituted cdMMP-14. Immobilized cdMMP-14 wt was incubated with Fabs (3A2, 3D9, and DX-2400 at 10 nM; 3E2, 2B5, and 3E9 at 20 nM) in the presence of 1 nM to 3 μM cdMMP-14 mutants. Captured Fabs were detected with anti-Fab-HRP for signal development. Four scenarios were observed. (A) Binding was abolished with the cdMMP-14 mutant. (B) The binding affinity was weakened with the mutant compared to cdMMP-14 wt. (C) The binding affinity was unchanged. (D) The binding affinity was enhanced with the cdMMP-14 mutant.

	cdMMP-14 Mutant	3A2		3E2		3D9		2B5		3E9		DX-2400	
		IC_{50}	ΔΔG	IC_{50}	ΔΔG	IC_{50}	ΔΔG	IC_{50}	ΔΔG	IC_{50}	ΔΔG	IC_{50}	ΔΔG
	WT	48	-	15	-	130	-	70	-	48	-	58	-
160s	Y166A	54	0.07	20	0.17	56	-0.50	22	-0.69	10	-0.93	27	-0.45
160s	R168A	48	0.00	65	0.87	56	-0.50	22	-0.69	18	-0.58	38	-0.25
160s	E169A	156	0.70	20	0.17	60	-0.46	44	-0.27	11	-0.87	38	-0.25
190s	S189A	53	0.06	24	0.28	120	-0.05	56	-0.13	39	-0.12	51	-0.08
190s	T190A	43	-0.07	45	0.65	45	-0.63	25	-0.61	40	-0.11	50	-0.09
190s	D193A	1020	1.81	60	0.82	760	1.05	350	0.95	66	0.19	240	0.84
190s	E195A	430	1.30	95	1.09	270	0.43	320	0.90	15	-0.69	200	0.73
190s	F198A	21	-0.49	920	2.43	74	-0.33	32	-0.46	48	0.0	22	-0.57
200s	Y203A	26	-0.36	18	0.11	130	0.00	32	-0.46	55	0.08	35	-0.30
200s	F204A	39	-0.12	15	0.00	450	0.73	38	-0.36	40	-0.11	29	-0.41
200s	I209A	45	-0.04	12	-0.13	170	0.16	49	-0.21	28	0.32	68	0.09
230s	N229A	140	0.63	50	0.71	200	0.25	120	0.32	11	-0.87	140	0.52
230s	N231A	51	0.04	15	0.00	45	-0.63	1000	1.57	95	0.40	93	0.28
230s	V236A	48	0.00	40	0.58	110	-0.10	56	-0.13	7.6	-1.09	48	-0.11
250s	S250A	180	0.78	22	0.23	160	0.12	61	-0.08	37	-0.15	77	0.17
250s	S251A	67	0.20	110	1.18	130	0.00	64	-0.05	11	-0.87	80	0.19
250s	D252A	48	0.00	40	0.58	63	-0.43	48	-0.22	7.6	-1.09	64	0.06
260s	P259A	82	0.31	1000	2.49	34	-0.79	40	-0.33	29	-0.30	24	-0.52
260s	F260A	-	-	140	1.32	74	-0.33	45	-0.26	1600	2.08	93	0.28
260s	Y261A	360	1.19	150	1.36	91	-0.21	200	0.62	13	-0.77	170	0.64

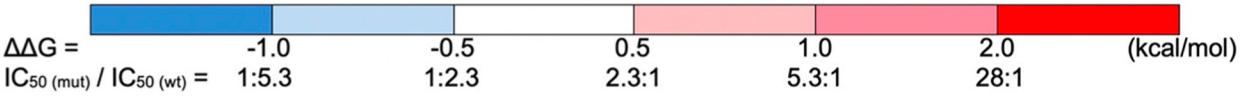

Figure 5.

Gibbs free energy changes (ΔΔ*G*) upon binding with mutant cdMMP-14 over wt. Values of IC_{50} (nanomolar) were measured by a competitive ELISA, and $\Delta\Delta G_{(\text{mut-wt})}$ (kilocalories per mole) values were calculated by the equation $\Delta\Delta G = RT \ln \frac{IC_{50(\text{Ala mutant})}}{IC_{50(\text{wild type})}}$, where $R = 1.987$ cal K^{-1} mol^{-1} and $T = 298$ K. A positive ΔΔ*G* (>0.5 kcal/mol, red) indicates that the binding affinity is weakened with the mutant; a negative ΔΔ*G* (less than −0.5 kcal/mol, blue) indicates that the binding affinity is enhanced with the mutant, and a |ΔΔ*G*| of <0.5 kcal/mol (white) suggests a nonsignificant change.

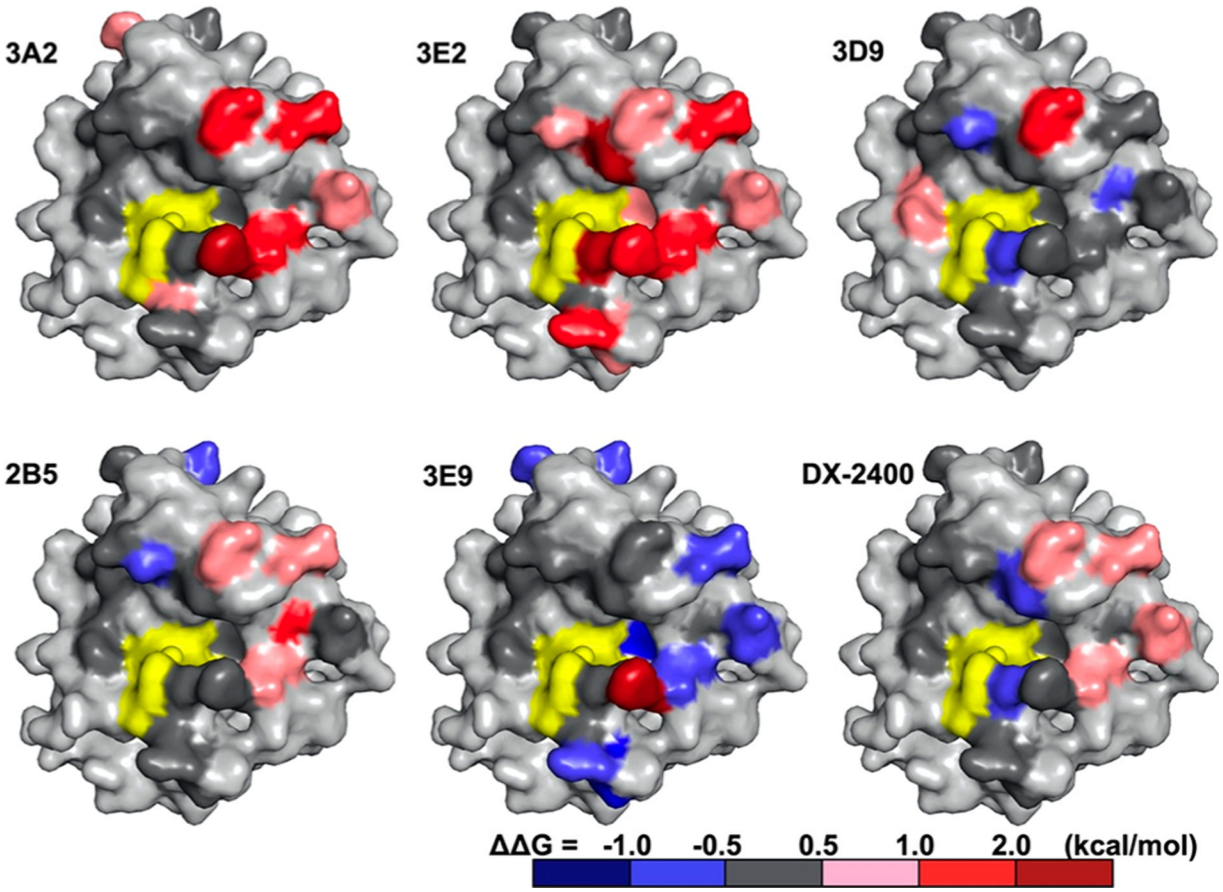

Figure 6.

Epitope mapping by alanine scanning mutagenesis. Point mutants that had a positive $\Delta\Delta G_{(mut-wt)}$ (increased IC_{50}) are colored pink (0.5–1.0 kcal/mol), red (1.0–2.0 kcal/mol), and brown (>2.0 kcal/mol), and mutants that had a negative $\Delta\Delta G_{(mut-wt)}$ (decreased IC_{50}) are colored blue. Point mutants that had a minimal effect on IC_{50} [$|\Delta\Delta G_{(mut-wt)}| < 0.5$ kcal/mol] are colored gray. The space-filling models are oriented in the same manner as in Figure 3, with the catalytic center colored yellow.

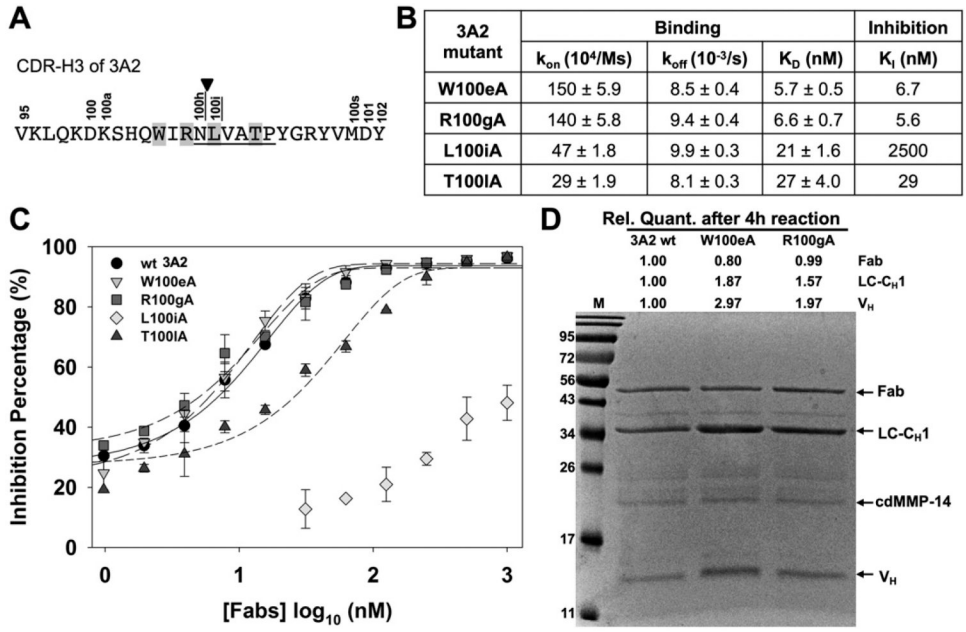

3A2 mutant	Binding			Inhibition
	k_{on} (10^4/Ms)	k_{off} (10^{-3}/s)	K_D (nM)	K_I (nM)
W100eA	150 ± 5.9	8.5 ± 0.4	5.7 ± 0.5	6.7
R100gA	140 ± 5.8	9.4 ± 0.4	6.6 ± 0.7	5.6
L100iA	47 ± 1.8	9.9 ± 0.3	21 ± 1.6	2500
T100IA	29 ± 1.9	8.1 ± 0.3	27 ± 4.0	29

Figure 7.

Characterizations of Fab 3A2 alanine point mutants. (A) CDR-H3 amino acid sequence of 3A2, showing the residues that match with the MMP-14 preferred substrate sequences (underlined, positions P1–P5′), cleavage site (arrowhead), and paratope positions chosen for alanine substitution (highlighted). (B) Binding kinetics and inhibitory potency data of 3A2 mutants. (C) Dose–response curves of inhibition measured with 30 nM cdMMP-14 and 1 μM FRET peptide substrate M-2350. (D) Fab stability assays with 3A2 wt and mutants W100eA and R100gA. Purified Fabs (2 μM) were incubated with 2 μM cdMMP-14 in 50 mM HEPES and 150 mM NaCl (pH 7.5) at 37 °C for 4 h and then analyzed by SDS–PAGE.

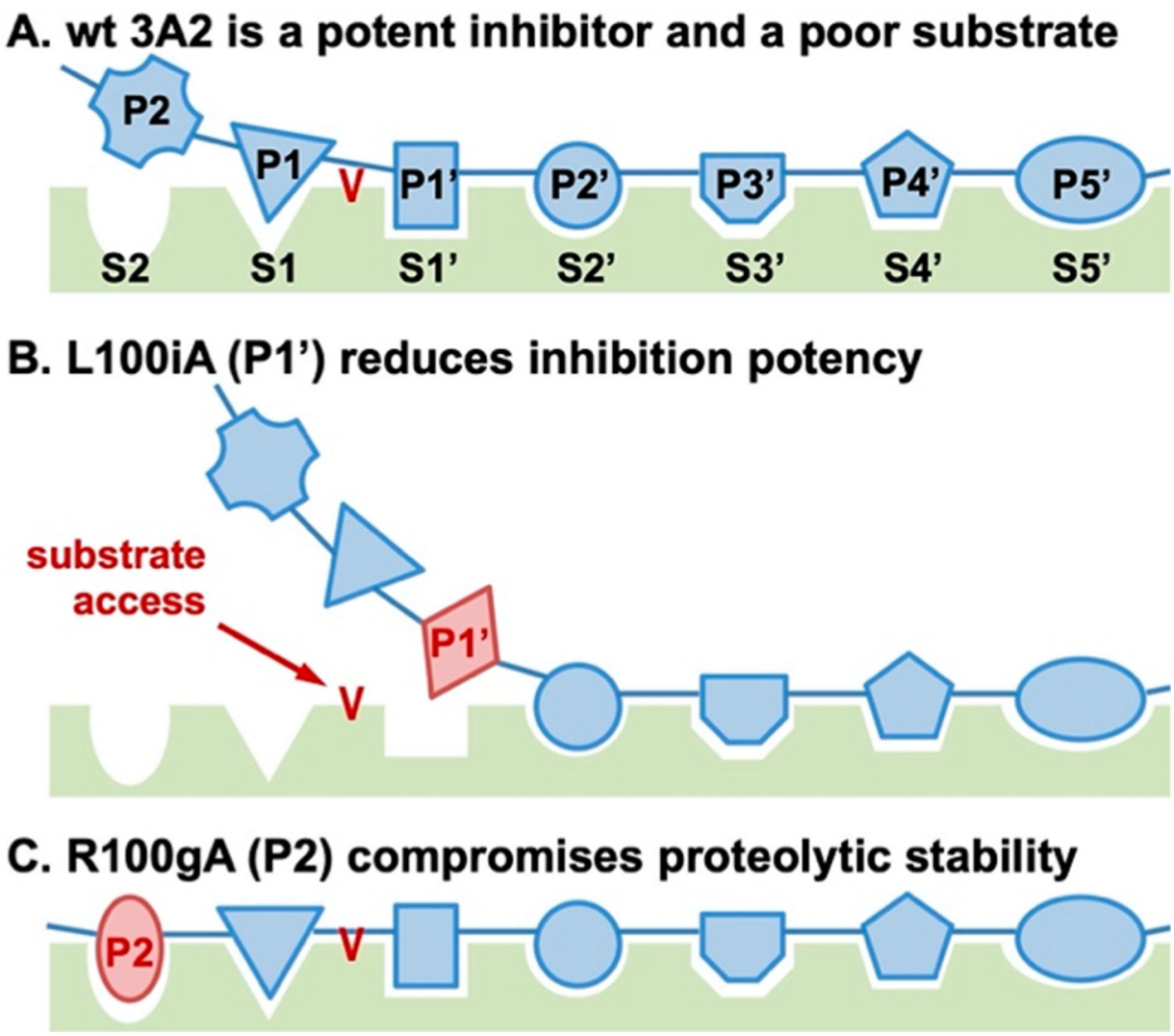

Figure 8.

Schematic drawing of the mechanism of inhibition of 3A2. (A) 3A2 is a canonical inhibitor recognizing MMP-14 subsites mainly via the prime portion with its CDR-H3. (B) Paratope alanine substitutions at the prime side, e.g., L100iA at P1′, weaken the inhibitory potency. (C) Paratope alanine substitutions at the nonprime side, e.g., R100gA at P2, compromise proteolytic stability.

Table 1.

Characterization of MMP-14 Inhibitory Fabs

		binding			inhibition		competitive ELISA	
Fab[a]	**CDR-H3 (length)**	**k_{on} ($\times 10^4$ M^{-1} s^{-1})**	**k_{off} ($\times 10^{-3}$ s^{-1})**	**K_D (nM)**	**K_I (nM)**	**mode**	**with nTIMP-2**	**with GM6001**
3A2	VKLQKDKSHQWIRNLVATPYGRYVMDY(27)	58 ± 2.2	4.3 ± 0.2	7.5 ± 0.7	8.7	competitive	competitive	not competitive
3E2	GIKGLVFTGSQMKMLRRGNYNWYVMDY(27)	29 ± 1.4	7.5 ± 0.3	26 ± 2.3	38	competitive	competitive	not competitive
3D9	RLMAYHGSCSSRLCQTAISPQRYAMDY(27)	68 ± 2.8	12 ± 0.4	18 ± 1.6	55	mixed	competitive	not competitive
2B5	IGVNAWAVKMSQRMLATRGSGWYVMDY(27)	13 ± 1.1	6.1 ± 0.3	45 ± 8.8	220	mixed	competitive	not competitive
3E9	NGRYPGFLKRAHKRLLNFKAYVMDY(25)	14 ± 1.4	6.1 ± 0.2	44 ± 5.7	5400	nd[c]	competitive	not competitive
DX-2400[b]	GRAFDI(6)	nd[c]	nd[c]	1.9[d]	4.3	competitive	competitive	not competitive

[a] From ref 33.

[b] From ref 23.

[c] Not determined.

[d] EC_{50} determined by an ELISA.